Advanced Design and Operation Consideration for Close-Connected Winding Permanent-Magnet Brushless DC Machine

Li Zhu, Shuangxia Niu, Y. C. Wang, and Chengmin Wang

***Abstract*—Advanced design and operation consideration for the close-connected winding permanent-magnet brushless DC machine is proposed in this paper, including circulating current elimination, fault-tolerant control for the breakdown of a power electronic switch, and a sensorless control method. With the finite-element analysis, the influence of machine design parameters on circulating current is investigated. By properly controlling the status of power electronic switches, the coils being connected into the equivalent circuit can be changed to avoid the failure switch. Sensorless control is explored by detecting the zero-crossing point of electromotive force.**

***Index Terms*—Circulating current, close-connected winding, fault-tolerant control, sensorless control.**

I. Introduction

THE close-connected winding permanent-magnet (PM) brushless DC machine has PM excitation, electric commutation, close-connected winding, and the operation principle of the machine is the same as a brushed DC machine [1]. Therefore, it is attractive for high torque density and high efficiency [1]–[3]. In this paper, advanced design and control consideration for the close-connected winding PM brushless DC machine is proposed [4]–[8], including circulating current elimination, fault tolerant control and sensorless control.

As the adoption of close-connected winding, the circulating current will occur. To decrease or even eliminate the circulating current, the influence of design parameters on the circulating current are studied with finite-element analysis (FEA).

Fault tolerant control is carried on for the breakdown of power electronic switches. By properly controlling the status of power electronic switches, the failure switch can be avoided and the coils connected into the equivalent circuit are changed.

This work was supported in part by the National Natural Science Foundation of China under Grant 51107082 and in part by the Hong Kong Research Grants Council, Hong Kong Special Administrative Region, China, through Project PolyU 5388/13E and Project 152130/14E.

L. Zhu is with Shanghai Jiao Tong University, Shanghai 200240, China, and also with Hong Kong Polytechnic University, Kowloon, Hong Kong (e-mail: L.Zhu@sjtu.edu.cn).

S. Niu and Y. C. Wang are with Hong Kong Polytechnic University, Kowloon, Hong Kong (e-mail: eesxniu@polyu.edu.hk; wangycee@gmail.com).

C. Wang is with Shanghai Jiao Tong University, Shanghai 200240, China (e-mail: wangchengmin@sjtu.edu.cn).

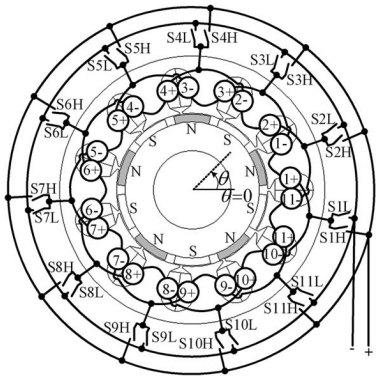

Fig. 1. Structure of the 10-pole and 11-slot close-connected winding PM brushless DC machine.

TABLE I
Machine Parameters

Rated power	200W	Rated voltage	48V
Rated speed	220rpm	Rated load	8Nm
Stator outer diameter	138mm	Stator inner diameter	80mm
Stator axial length	100mm	Mechanical air gap	0.5mm
Thickness of PMs	4mm	Magnet remanence	1.14T
PM relative recoil permeability	1.07	Pole-arc coefficient	0.7175
Height of slot opening	1mm	Height of slot shoulder	1mm

By detecting zero crossing point of electromotive force (EMF) for the particular coil which requiring current commutation, sensorless control is explored and realized

II. Machine Structure [1]

Fig. 1 is a close-connected winding PM brushless DC machine with 10-pole and 11-slot. The technical parameters of the machine are in Table I. Besides PM excitation and electric commutation, the machine has close-connected winding. The PMs are mounted on rotor, and armature windings on stator. In Fig. 1, θ is the mechanical angle along circumference, $i+$ and $i-$ $(i = 1, 2, \ldots, 11)$ are respectively the upper side and lower side of the ith coil. SiL and SiH $(i = 1, 2, \ldots, 11)$ are the power electric switches. The rotor rotation direction is anticlockwise, and α is the mechanical position angle of rotor, and $\alpha = 0$ in Fig. 1. α_e is the electrical position angle of rotor. The corresponding commutation circuit is shown in Fig. 2. By properly controlling the power electric switch status, the current direction under N or S pole keeps unchanged, just as the operation principle of brushed DC machine.

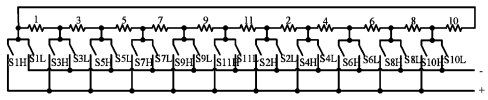

Fig. 2. Current commutation circuit of the machine in Fig. 1.

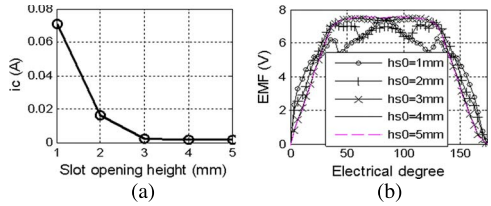

Fig. 3. (a) Influence of slot opening height on circulating current ($h_{s1} = 1$ mm). (b) EMF of coil with various slot opening height values ($h_{s1} = 1$ mm).

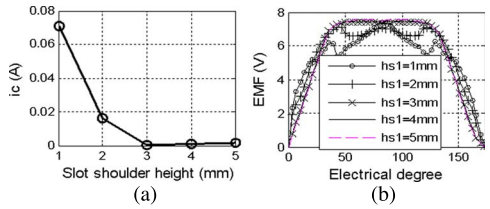

Fig. 4. (a) Influence of slot shoulder height on circulating current ($h_{s0} = 1$ mm). (b) EMF of coil with various slot opening height values ($h_{s0} = 1$ mm).

III. Circulating Current Elimination

As the close-connected winding, circulating current may be caused between different current branches, that is

$$i_c = \max(i_{\mathrm{ck}}) \quad (k = 1, 2, \ldots, a-1) \tag{1}$$

where α is the current branch number of close-connected winding PM brushless DC machine, and i_{ck} is the circulating current between the kth and $k+1$th current branches. It is

$$i_{\mathrm{ck}} = \max\left(abs \left| \frac{\sum\limits_{k,k+1} e(\alpha)}{\sum\limits_{k,k+1} R} \right| \right) \tag{2}$$

where e and R are respectively EMF and resistance of a coil, and k and $k+1$ represent the kth and $k+1$th current branch.

According to Eq. (1), the influence of design parameters on the circulating current can be analyzed with FEA. Figs. 3–8 show the influences of design parameters on circulating current when the rotation speed is 200 rpm. In Figures, α_p is pole-arc coefficient, h_{s0} is height of slot opening, h_{s1} is height of slot shoulder, b_{s0} is width of slot opening and N_S is slot number.

Fig. 3 is the influence of slot opening height on circulating current with $h_{s1} = 1$ mm. In Fig. 3(a), with the increase of h_{s0}, the circulating current decreases sharply. If h_{s0} is higher than 3 mm, the increase of h_{s0} has no effect on the circulating current. It is because the EMF waveform of coil is distorted rather than flat top waveform as in Fig. 3(b), when h_{s0} is small and the tooth tip is highly saturated. When the tooth tip is not saturated, the increase of h_{s0} has little effect on the coil's EMF.

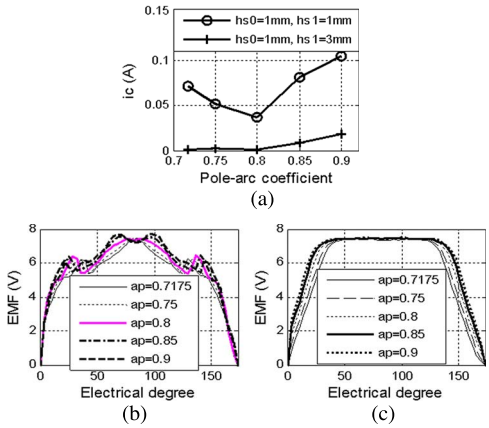

Fig. 5. (a) Influence of pole-arc coefficient on circulating current. (b) EMF of coil with various pole-arc coefficients ($h_{s0} = 1$ mm, $h_{s1} = 1$ mm). (c) EMF of coil with various pole-arc coefficients ($h_{s0} = 1$ mm, $h_{s1} = 3$ mm).

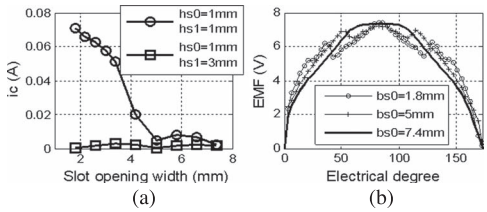

Fig. 6. (a) Influence of slot opening width on circulating current. (b) EMF of coil with various slot opening width values ($h_{s0} = 1$ mm, $h_{s1} = 1$ mm).

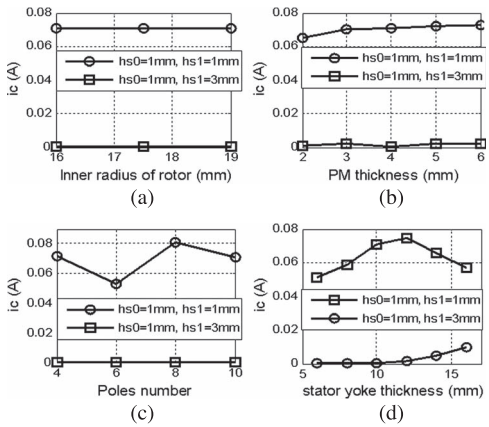

Fig. 7. (a) Influence of rotor yoke on circulating current. (b) Influence of PM thickness on circulating current. (c) Influence of pole number on circulating current. (c) Influence of stator yoke thickness on circulating current.

Fig. 4 is the influence of slot shoulder height on circulating current when $h_{s0} = 1$ mm. From Fig. 4, the influence of slot shoulder height on circulating current is very similar to the influence of slot opening height as in Fig. 3.

Fig. 5 is the influence of pole-arc coefficient on circulating current. According to Fig. 5(a), when the tooth tip is saturated ($h_{s0} = 1$ mm, $h_{s1} = 1$ mm), the circulating current is smallest at $\alpha_p = 0.8$ because the coil's EMF waveform is relatively best at $\alpha_p = 0.8$ in Fig. 5(b). If the tooth tip is unsaturated ($h_{s0} = 1$ mm, $h_{s1} = 3$ mm), the circulating current is much smaller and α_p almost has no effect on circulating current, because of the flat top EMF waveform as in Fig. 5(c).

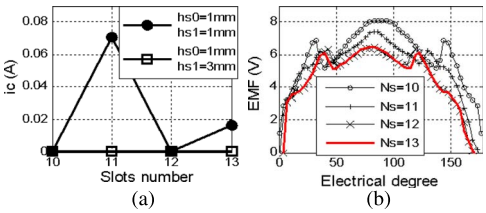

Fig. 8. (a) Influence of slot number on circulating current. (b) EMF of coil with various slot numbers ($h_{s0} = 1$ mm, $h_{s1} = 3$ mm).

In Fig. 6(a), the width of slot opening has no influence on circulating current with $h_{s0} = 1$ mm and $h_{s1} = 3$ mm, because of no saturation in tooth tip. With $h_{s0} = 1$ mm and $h_{s1} = 1$ mm, the increase of b_{s0} can make the circulating current decrease. When the tooth width is kept unchanged, the increase of b_{s0} makes the tooth tip shorter, and the tooth tip becomes unsaturated and then the coil's EMF waveform is with flat top as in Fig. 6(b).

From Fig. 7(a) and (b), rotor yoke thickness and PM thickness has no effect on circulating current. From Fig. 7(c) and (d), poles number and stator yoke thickness have little effect on circulating current.

In Fig. 8(a), slot number has no effect on circulating current, when tooth tip is unsaturated and coil's EMF waveform has flat top with $h_{s0} = 1$ mm and $h_{s1} = 3$ mm. However, with $h_{s0} = 1$ mm and $h_{s1} = 1$ mm, even slot number can eliminate circulating current even with distorted coil's EMF waveform as in Fig. 8(b).

Therefore, according to Figs. 3–8, to decrease or eliminate the circulating current, the new machine should be designed with flat top EMF waveform or even slot number.

IV. Fault Tolerant Control

Normally, for the prototype of 10-pole and 11-slot machine in Fig. 1, when the rotor rotates through 2π electric degree, every switch is only being on for $2\pi/N_S$ electric degree. For example, about the power electric switch $S1H$, $S1H$ and $S2L$ are being on at $\alpha_e = 0 \sim \pi/N_S$, and $S1H$ and $S11L$ are being on at $\alpha_e = \pi/N_S \sim 2\pi/N_S$. Then, $S1H$ is off during the remaining rotation position of 2π electric degree.

In normal condition, at $\alpha_e = 0 \sim \pi/N_S$, according to the coils' position under N or S pole, $S1H$ and $S2L$ are turned on. Coil 1, 3, 5, 7, 9, and 11 compose one current branch, coil 2, 4, 6, 8, and 10 compose the other current branch. The EMFs of the coils satisfy

$$(e_1+e_3+e_5+e_7+e_9+e_{11})+(e_2+e_4+e_6+e_8+e_{10})=0. \tag{3}$$

Similarly, at $\alpha_e = \pi/N_S \sim 2\pi/N_S$, $S1H$ and $S11L$ are turned on. Coil 1, 3, 5, 7, and 9 are in one current branch, coil 11, 2, 4, 6, 8, and 10 are in the other current branch, and there is

$$(e_1+e_3+e_5+e_7+e_9)+(e_{11}+e_2+e_4+e_6+e_8+e_{10})=0. \tag{4}$$

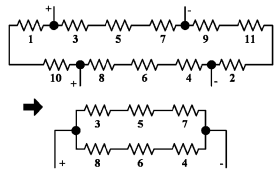

Fig. 9. Equivalent circuit at $\alpha = 0$, $S10H$, $S4L$, $S3H$, and $S9L$ are on.

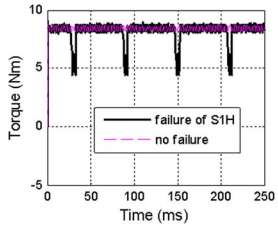

Fig. 10. FEA-simulated torque when $S1H$ is failure (200 r/min, $I_{\rm DC} = 5$ A).

With Fig. 1, at $\alpha_e = 0 \sim \pi/N_S$, there are $e_{11} \approx 0$, $e_1 + e_{11} \approx 0$, and $e_2 + e_9 \approx 0$. Then, Eq. (3) can be expressed as

$$\begin{cases} (e_3 + e_5 + e_7) + (e_4 + e_6 + e_8) \approx 0 \\ e_1 + e_{10} \approx 0 \\ e_9 + e_{11} + e_2 \approx 0. \end{cases} \tag{5}$$

According to (5) and Fig. 2, at $\alpha_e = 0 \sim \pi/N_S$, $S10H$, $S4L$, $S3H$, and $S9L$ can be turned on if $S1H$ is failure. Coils 3, 5, and 7 are in one current branch. Coils 4, 6, and 8 are in the other current branch. Serial coils 1 and 10, and serial coils 9, 11, and 2 are not in the equivalent circuit, as shown in Fig. 9. Similarly, at $\alpha_e = \pi/N_S \sim 2\pi/N_S$, there is

$$\begin{cases} (e_3 + e_5 + e_7) + (e_2 + e_4 + e_6) \approx 0 \\ e_9 + e_{11} \approx 0 \\ e_1 + e_{10} + e_8 \approx 0. \end{cases} \tag{6}$$

$S8H$, $S2L$, $S3H$, and $S9L$ are turned on according to Fig. 2 if $S1H$ is failure. Coils 3, 5, and 7 are in one current branch. Coils 2, 4, and 6 are in the other current branch. Serial coils 1, 10, and 8, and serial coils 9 and 11 are not in the equivalent circuit.

Therefore, If $S1H$ is with open-circuit failure, the machine can still be kept running. Fig. 10 is the FEA simulation result for output torque when the rotation speed is 200 rpm and input DC current is 5 A. Therefore, although the failure of power switch will cause torque fluctuation because of less coils in the equivalent circuit, the machine can still keep running. Similarly, by properly controlling the status of switches, fault-tolerant control can be realized for other failure switches.

V. Sensorless Control

Zero-crossing detection of back EMF is now explored for sensorless control of the close-connected PM brushless DC machine. The voltage of the nth coil is

$$v_n = e_n + L\frac{di_n}{dt} + Ri_n + \sum_{m \neq n} M_{\rm mn}\frac{di_m}{dt} \tag{7}$$

(a) (b)

Fig. 11. Stator and rotor of the 10-pole and 11-slot prototype machine. (a) Stator. (b) Rotor.

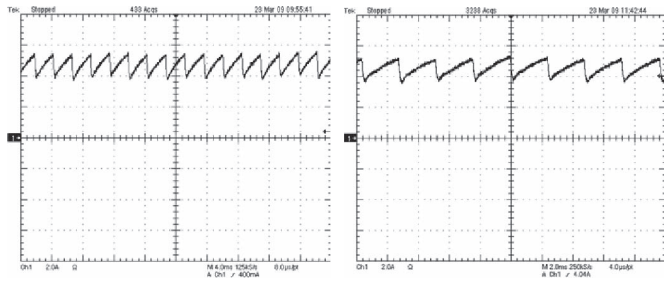

(a) (b)

Fig. 12. Current waveform with experiments (8 Nm, 225 r/min). (a) Sensor control (2 A/div, 4 ms/div). (b) Sensorless control (2 A/div, 2 ms/div).

where L is the self-inductance of the coil, and $M_{\rm mn}$ is the mutual-inductance between the mth coil and nth coil. As the operation principle of the close-connected winding PM brushless DC machine is identical to traditional DC machine, the current of coil is DC. Therefore, for simplicity, it is assumed $di/dt = 0$. Then, Eq. (3) can be rewritten as

$$v_k = e_k + Ri_k. \tag{8}$$

If the EMF of the coil is zero-crossing, the voltage of the coil is

$$v_k = Ri_k. \tag{9}$$

Therefore, if the voltage of coil satisfies (9), the zero-crossing point of EMF can be detected for electric current commutation.

For the machine in Fig. 1, $S1H$ and $S2L$ are turned on at $\alpha_e = 0$, and there are current branch 1-3-5-7-9-11 under S pole and current branch 10-8-6-4-2 under N pole. When the rotor rotates to $\alpha_e = \pi/N_S = \pi/11$, the position of coil 11 changes from S pole to N pole. Coil 1,3, 5, 7, 9 are under S pole and coil 10, 8, 6, 4, 2, 11 are under N pole. Therefore, $S1H$ and $S11L$ are turned on for the current branch 1-3-5-7-9 and current branch 10-8-6-4-2-11. When the rotor rotates to $\alpha_e = 2\pi/N_S = 2\pi/11$, the position of coil 10 changes form S pole to N pole. $S10H$ and $S11L$ should be turned on for current branch 10-1-3-5-7-9 under S pole and current branch 8-6-4-2-11 under N pole. Similarly, if the position of a coil under N or S pole changes, the switch status should be renewed to keep the coils under N pole in the same current branch and coils under S pole in another current branch.

Therefore, at $\alpha = 0$ and $S1H$ and $S2L$ turned on, the voltage of coil 11 is being detected for the EMF zero-crossing point according to (9). When the EMF of coil 11 has the zero-crossing point, $S1H$ and $S11L$ are turned on and the voltage of coil 10 is begin to be detected for the EMF zero-crossing point with (9). If the EMF zero-crossing point of coil 10 occurs, $S10H$ and $S11L$ are turned on, and the voltage of coil 9 is begin to be detected for the EMF zero-crossing point to keep the machine running. Similarly, by detecting the EMF cross-point of a certain coil at different control state, the sensorless control can be realized for the close-connected winding PM brushless DC machine.

The prototype machine is shown in Fig. 11. Fig. 12 are the measured current waveforms of experiments respectively with sensor and sensorless control. The current of sensorless control is very similar to that of sensor control in Fig. 12.

VI. Conclusion

Advanced design and control consideration for the close-connected winding PM brushless DC machine is studied. To decrease or eliminate the circulating current, flat top EMF waveform or even slot number should be particularly designed. By properly controlling the status of switches, the failure switches can be avoided and the machine keeps running. While, as with less coils in the equivalent circuit, the fault-tolerant control may cause torque or speed fluctuation. Sensorless control based on zero-crossing detection of back EMF is very effectual and the performance is the same as sensor control.

References

[1] L. Zhu, S. Z. Jiang, Z. Q. Zhu, and C. C. Chan, "A new simplex wave winding permanent-magnet brushless DC machine," *IEEE Trans. Magn.*, vol. 47, no. 1, pp. 252–259, Jan. 2011.

[2] C. Liu, K. T. Chau, J. Zhong, and J. Li, "Design and analysis of a HTS brushless doubly-fed doubly-salient machine," *IEEE Trans. Appl. Supercond.*, vol. 21, no. 3, pp. 1119–1122, Jun. 2011.

[3] C. Liu, K. T. Chau, J. Zhong, W. Li, and F. Li, "Quantitative compassion of double-stator permanent magnet vernier machines with and without HTS bulks," *IEEE Trans. Appl. Supercond.*, vol. 22, no. 3, Jun. 2012, Art. no. 520240.

[4] D. Yao and D. M. Ionel, "A review of recent developments in electrical machine design optimization methods with a permanent magnet synchronous motor benchmark study," *IEEE Trans. Ind. Appl.*, vol. 49, no. 3, pp. 1268–1275, Sep. 2013.

[5] G. Lei, T. S. Wang, Y. G. Guo, J. G. Zhu, and S. H. Wang, "System level design optimization methods for electrical drive systems: Deterministic approach," *IEEE Trans. Ind. Electron.*, vol. 61, no. 12, pp. 6591–6602, Dec. 2014.

[6] G. Lei *et al.*, "Techniques for multilevel design optimization of permanent magnet motors," *IEEE Trans. Energy Conver.*, vol. 30, no. 4, pp. 1574–1584, Nov. 2015.

[7] H. M. Hasanien, "Particle swarm design optimization of transverse flux linear motor for weight reduction and improvement of thrust force," *IEEE Trans. Ind. Electron.*, vol. 58, no. 9, pp. 4048–4056, Sep. 2011.

[8] Q. F. Teng, J. G. Zhu, T. S. Wang, and G. Lei, "Fault tolerant direct torque control of three-phase permanent magnet synchronous motors," *WSEAS Trans. Syst.*, vol. 8, no. 11, pp. 465–476, Jan. 2012.